6-5-2013

V-band bandpass filter with continuously variable centre frequency

Dimitra Psychogiou
Swiss Federal Institute of Technology Zurich

Dimitrios Peroulis
Birck Nanotechnology Center, Purdue University, dperouli@purdue.edu

Yunjia Li
Swiss Federal Institute of Technology Zurich

Christian Hafner
Swiss Federal Institute of Technology Zurich

Published in IET Microwaves, Antennas & Propagation
Received on 22nd December 2012
Revised on 22nd March 2013
Accepted on 1st April 2013
doi: 10.1049/iet-map.2012.0722

ISSN 1751-8725

V-band bandpass filter with continuously variable centre frequency

Dimitra Psychogiou[1], Dimitrios Peroulis[2], Yunjia Li[3], Christian Hafner[1]

[1]*Laboratory for Electromagnetic Fields and Microwave Electronics, Department of Information Technology and Electrical Engineering, ETH Zurich, 8092 Zürich, Switzerland*
[2]*School of Electrical and Computer Engineering, Birck Nanotechnology Center, Purdue University, West Lafayette, IN 47907, USA*
[3]*Group of Micro and Nanosystems, Department of Mechanical and Process Engineering, ETH Zurich, 8092 Zürich, Switzerland*
E-mail: pdimitra@ifh.ee.ethz.ch

Abstract: A second-order bandpass filter (BPF) with continuously variable centre frequency tuning is presented in this article. Evanescent-mode cavity resonators with variable capacitive loadings are used as tuning elements. Tuning is achieved by means of micro-electromechanical-systems (MEMS)-actuated highly conductive rigid fingers that feature an out-of-plane deflection. For an applied DC bias voltage between 0 and 27.3 V the centre frequency of the BPF is tuned from 67.4 to 63.2 GHz (4.2 GHz). For this frequency band, the fractional bandwidth (FBW) varies between 8.3 and 3.4% and the in-band insertion loss between 1.45 and 5 dB.

1 Introduction

There has been an increasing demand for wireless communication systems with broadband and high data-rate (> 2 Gb/s) transmission characteristics to accommodate applications such as gigabit Ethernet and high-speed internet, automotive and radar sensing, real-time video streaming and high-definition television. The recently released unlicensed 60 GHz-frequency zone of V-band (50–75 GHz) is well suited for these applications because of the advantages of wide bandwidth, increased spatial resolution, compact integration and reduced interference that is enabled by the high attenuation of oxygen at those frequencies. V-band bandpass filters (BPFs) are fundamental components of the RF-front-end systems of the applications mentioned above. They can be utilised for pre-selection of the desired frequency band and rejection of the undesired interference and noise [1]. It has been reported elsewhere that BPFs with reconfigurable characteristics may enable transceiver modules with multi-frequency and multi-standard operation [2]. In addition, they may result in reduced cost and volume transceivers (compared with traditional implementation concepts that utilise filter banks). Thus, it is highly desirable to explore reconfigurable filter concepts for V-band applications.

V-band BPFs presented in the literature are primarily based on planar transmission line resonators (coplanar waveguide, microstrip) and show static operational characteristics [3–10]. They are mainly fabricated by complementary metal-oxide-semiconductor (CMOS) processes and feature an in-band insertion loss between 2 and 9 dB for fractional bandwidths (FBWs) between 10 and 30% [3–5]. Alternative integration concepts relate to low temperature co-fired ceramic (LTCC) substrates [9], silicon micromachining [10] liquid crystal polymer (LCP) substrates [7] and integrated passives technology (IPD) [8]. To the best of the authors' knowledge the number of existing tuneable V-band BPFs is relatively limited because of technological advances that are required for the co-integration of low loss tuneable elements such as RF-MEMS [1]. The first frequency reconfigurable V-band BPF was demonstrated in the open literature by Kim *et al.* in [11]. It was based on eight tuneable MEMS capacitors fabricated on a quartz substrate and showed a frequency tuning range of 10% (59–65.5 GHz) with an insertion loss between 3.1 and 3.5 dB. In a subsequent publication [2], Park *et al.* presented a broadband (60%) BPF operating up to the lower edge of V-band with two discrete tuning states (20 GHz and 55 GHz) obtained by four multiple-contact MEMS switches and coplanar waveguide (CPW)-transmission lines. Later on,Lucyszyn *et al.* [12] introduced a silicon micromachined inverted-microstrip BPF based on MEMS actuated cantilevers. The authors successfully demonstrated a tuneable resonator with limited tuning range (60.8–60.92) and Q_u (85–100). However, the obtained filter response was static and showed an insertion loss of about 3 dB at 59.7 GHz. An alternative tuning concept based on benzocyclobutene (BCB) flexible polymer substrates integrated on top of microstrip transmission line resonators was proposed by Seok *et al.* [13]. The authors showed a pass-band response between 63.34 and 64.9 GHz with an insertion loss between 9.4 and 9.7 dB obtained by static

measurements on multiple filters having BCB cap membranes on predefined heights (non-tuneable).

Evanescent-mode cavity resonators and filters have attracted considerable attention [14–17], because of their advantages towards miniature size, spurious-free response, high quality factor (compared with their half-wave counterparts) and high-power handling capabilities (compared with planar transmission lines). Hence, it can be envisioned that their co-integration with MEMS tuneable components may pave the way to outperforming reconfigurable devices for high-frequency applications. Topologies presented in the open literature utilise RF-MEMS as tuning elements, show relatively high tuning ranges (1.4:1 in [14] 1.55:1 in [16] and high unloaded quality factors (354–400 in [14] and 470–645 in [16]) but their operation is limited to frequencies up to 6 GHz. In [17], Arif *et al.* demonstrated a MEMS-actuated evanescent-mode cavity resonator with excellent RF performance (tuning range 4:1and Q of 300–1000) but only for frequencies up to 24 GHz.

In this paper, the authors demonstrate for the first time the implementation and experimental validation of a high-frequency (> 60 GHz) evanescent-mode resonator BPF with continuously variable centre frequency. The proposed concept is based on capacitively loaded resonators tuned by MEMS-actuated highly conductive rigid fingers that feature an out-of-plane deflection. An applied DC bias voltage between 0 and 27.3 V results in a centre frequency tuning from 67.4 to 63.2 GHz. For this frequency band the measured FBW varies between 8.3 and 3.4% and the in-band insertion loss is measured between 1.45 and 5 dB.

The organisation of this paper is as follows: In Section 2 the fundamental concept and the filter design are presented. In Section 3, the measured RF performance of a manufactured prototype is discussed.

2 Tuneable Bandpass Filter

2.1 Tuning concept

A 2nd-order BPF can be realised by two series cascaded resonators and appropriate external ($Q_{e1} = Q_{e2}$) and interresonator (K_{12}) coupling coefficients which are mainly defined by the desired frequency response (e.g. Butterworth, Chebyshev, etc.) and FBW. The centre frequency of a BPF can be then reconfigured by synchronously tuning the centre frequency of each resonator (1 and 2 in Fig. 1).

A realisation concept for a tuneable BPF using evanescent-mode cavity resonators is illustrated in Fig. 1. It consists of an evanescent-mode waveguide section (L) which comprises of five protruding studs, four notches and two highly-conductive rigid fingers. Each resonator is realised by a capacitive post (1, 2) located in the middle of an evanescent-mode rectangular cavity. The inter-resonator coupling coefficient (K_{12}) is mainly capacitive and created by the long stud (w_p, h_m, L_s) located in-between resonators 1 and 2 and the resonator separation ($2L_m + 2L_s$). The external coupling coefficient is obtained by the edge-post (w_p, h_e, L_s) in the waveguide-cavity and the distance between the resonator and the RF-input/output ($1.5L_s + L_e$). The centre frequency of each resonator can be effectively tuned by varying the capacitive gap g_r. This is achieved with the aid of two highly conductive rigid fingers that are integrated inside the waveguide bottom wall, Fig. 1. Their deflection (α) towards the resonator capacitive posts results

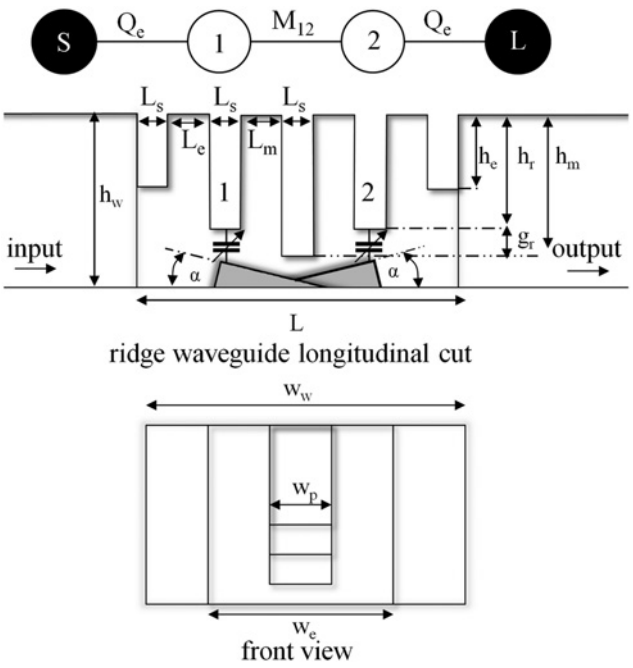

Fig. 1 *Tuneable BPF concept. For a design frequency around 68 GHz: $w_p = 0.5$ mm, $w_w = 2.5$ mm, $w_e = 1.43$ mm, $L_s = 0.2$ mm, $L_e = 0.4$ mm, $L_m = 0.25$ mm, $h_e = 0.65$ mm, $h_r = 0.805$ mm, $h_m = 0.965$ mm, $h_w = 1.1$ mm*

in a variable capacitive loading, which in turn results in a decrease of the centre frequency of the bandpass.

2.2 Waveguide filter design

For a second-order Butterworth BPF with 8% FBW, the coupling coefficients are calculated using the Butterworth second-order low-pass prototype in [18] ($Q_{ext1} = Q_{ext2} = 17.675$, $K_{12} = 0.057$). Full-wave simulations are performed with the aid of a finite element software ANSYS HFSS in order to define the resonator size and to correlate the

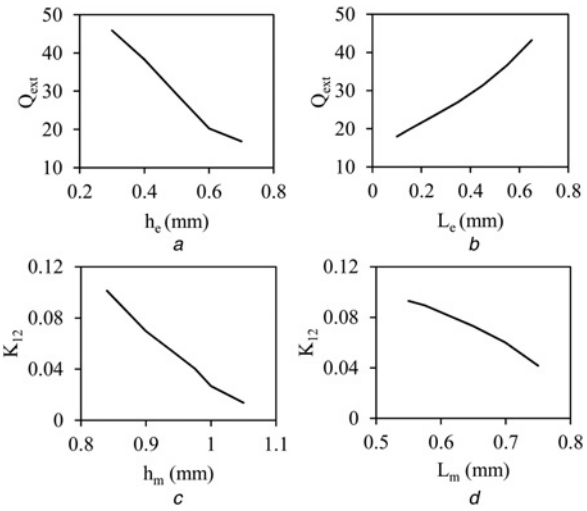

Fig. 2 *Calculated relationship between*

a Q_{ext} and h_e ($L_e = 0.4$ mm, $L_s = 0.2$ mm, $h_r = 0.805$ mm)
b Q_{ext} and L_e ($h_e = 0.5$ mm, $L_s = 0.2$ mm, $h_r = 0.805$ mm)
c K_{12} and h_m ($L_m = 0.25$ mm, $L_s = 0.2$ mm, $h_r = 0.805$ mm)
d K_{12} and L_m ($h_m = 0.8$ mm, $L_s = 0.2$ mm, $h_r = 0.805$ mm) for a frequency around 68 GHz

doi: 10.1049/iet-map.2012.0722

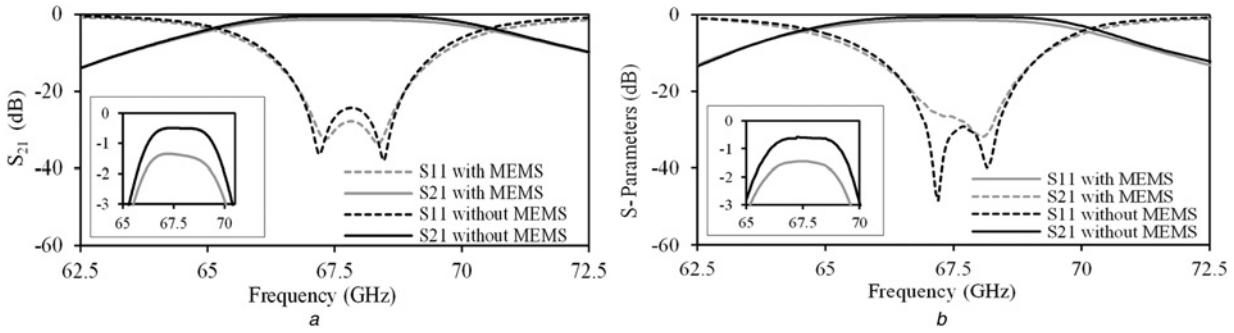

Fig. 3 *Simulated and measured S-parameters of the V-band BPF with and without MEMS tuner*

a Simulated S-parameters for a BPF with solid metal bottom wall (without MEMS) and with a MEMS tuner integrated inside the bottom wall (with MEMS)
b Measured S-parameters of a waveguide fixture that uses a solid brass plate as a ground plane and a waveguide fixture with the MEMS tuner integrated in the bottom wall without any applied DC bias voltage. Insets show the effect of MEMS integration in transmission response

required coupling coefficients (Q_{ext} and K_{12}) to the corresponding filter dimensions (as specified in Section 2.2) by using the filter synthesis method described in [18, 19]. Fig. 2 illustrates the relationship between each coupling coefficient and alternative geometrical parameters of the filter. For the initial filter design, the MEMS tuner is replaced by a solid conductive wall and initial dimensions for the coupling sections are obtained from Fig. 2. The optimised dimensions for a typical Butterworth BPF response (8% FBW) centred at frequency about 68 GHz are shown in Fig. 1. For brass, assumed as a material, the insertion loss of the filter is calculated about 0.5 dB, Fig. 3*a*

The numerical model that is utilised for the electromagnetic analysis of a practical implementation concept of the proposed filter is depicted in Fig. 4. It consists of the evanescent-mode waveguide filter, the MEMS tuner and two waveguide transitions. Each transition comprises of a quarter-wavelength transformer that allows the connection of the filter that has a rectangular cross section of 1.1 mm × 2.5 mm to a standard WR15 waveguide. The transition was optimised for frequencies between 61 and 75 GHz with an input reflection below -15 dB and insertion loss lower than 0.22 dB for brass assumed as a material.

In order to better evaluate the expected performance of the tuneable BPF the following material parameters need to be considered for the filter modelling. The waveguide upper and bottom part are modelled as metals with conductivity σ: 1.5×10^7 S/m (typical conductivity of brass). The MEMS tuner geometry [20, 21] is represented by a 4-layer geometry (a top metallisation layer and three silicon layers) with the following characteristics; device layer: ε_r: 11.7, ρ: 0.0063 Ω·cm, thickness: 80 μm, stator layer: ε_r: 11.7, ρ: 0.008 Ω·cm, thickness: 180 μm, handle layer: ε_r: 11.3, ρ: 9.1 Ω·cm, thickness: 400 μm. The MEMS top metallisation layer is modelled as a metal sheet with finite thickness about 500 nm and conductivity σ: 4.1×10^7 S/m (typical conductivity of gold). A solve-inside mesh option needs to be selected so as to account for the conductive losses because of the skin depth effect. The SU8-spring is represented as a dielectric material with ε_r: 4.2 and tanδ: 0.02.

The simulated filter performance is shown in Figs. 5*a* and *b*. Fingers deflections between 0 and 8.5° (g_r: 295 μm–105 μm) result in a BPF response with variable centre frequency from 67.8 to 63.8 GHz (4 GHz). For this frequency range the FBW varies between 8.3 and 4.5% and the in-band insertion loss (IL, calculated as $-10 \log (S_{21})^2$) varies between 1.6 and 2.92 dB (including the loss of the waveguide transition), Fig. 5*e*.The integration of the MEMS tuner (α = 0°) inside the waveguide bottom wall results in small centre frequency (from 68 to 67.8 GHz) and FBW shifts (from 8 to 8.3%) compared with the performance of the initial filter design in which a solid metal wall was utilised. On the other hand, it results in increased insertion loss (1.6 dB instead of 0.5 dB that was calculated for the filter with a solid metal wall), Fig. 3*a*. This can be attributed to increased conductive losses because of the interaction of the surface currents with the MEMS tuner geometry which is made out

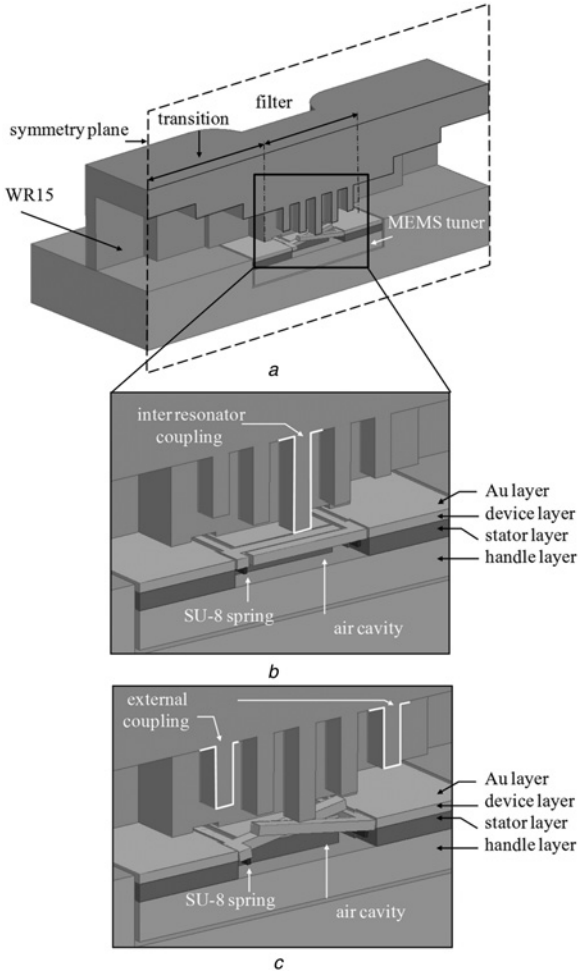

Fig. 4 *Implementation concept of a tuneable V-band BPF*

a Conceptual drawing of the tuneable BPF numerical model
b Tilting fingers at 0° deflection
c Tilting fingers at 8.5° deflection

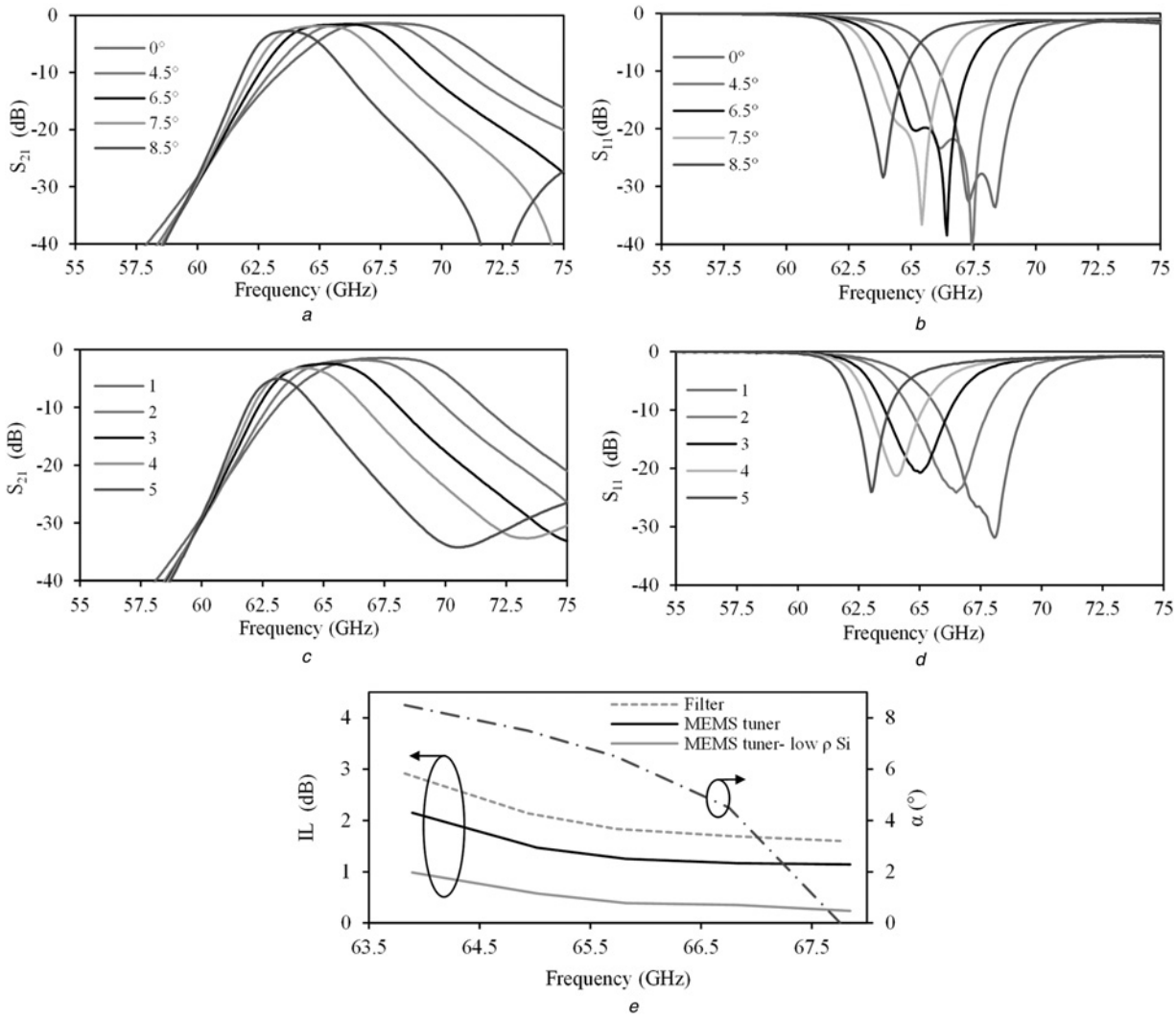

Fig. 5 *Simulated amd measured S-parameters of the tuneable V-band BPF*

a Simulated transmission (S_{21}) for various sets of deflection angles between 0 and 8.5°
b Simulated input reflection (S_{11}) for the same angles shown in (a)
c Measured transmission (S_{21}) for various set of biasing voltages where state 1 corresponds to 0 V (α: 0.3°) and state 5 to 23.7 V (α: 8.3°)
d Measured input reflection (S_{11}) for the same biasing states shown in (c)
e Simulated insertion loss for the filter and for MEMS tuners with different material parameters

of poor conductive materials. (thin Au metallisation layer and low resistivity silicon). In addition, all slots around the MEMS fingers and in particular the ones perpendicular to the surface current direction act as discontinuities and contribute to the loss.

Simulation allows for the evaluation of the loss because of the MEMS tuner for different deflection states; and was calculated between 1.14 (for $\alpha = 0°$) and 2.15 dB (for $\alpha = 8.5°$), Fig. 5*e*. It can be observed that insertion loss grows towards higher deflections because of increased current densities that appear for smaller capacitive gaps g_r and result in excessive conductive loss. Furthermore, the current leakage to the MEMS substrate becomes larger for higher deflections because of the open air cavity inside the stator substrate (Fig. 4*b* and *c*) that increases with deflection and acts as discontinuity enabling part of the RF signal to leak in the stator and handle layer. The loss contribution because of the MEMS tuner can be improved if silicon with very low resistivity is utilised as structural material for the MEMS tuner. An example of a MEMS tuner consisting of three layers of Si with ρ: 0.0025 Ω·cm and 500 nm-thick Au top metallisation is shown in Fig. 5*e* to improve the loss arising from the tuner for all tuning states (e.g. from 1.14 to 0.24 dB for $\alpha = 0°$ and from 2.15 to 1 dB for $\alpha = 8.5°$).

3 Measurements and discussion

3.1 RF-measurements

Fig. 6 illustrates the manufactured prototype that was built and measured for the experimental validation of the proposed filter concept. It is based on a split-block approach and consists of three metal parts (upper part, bottom part and waveguide) and a MEMS tuner that comprises of two antiparallel-oriented highly conductive rigid fingers. For the fabrication of the waveguide metal parts high-precision milling was utilised. The MEMS tuner fabrication was performed with a bulk-silicon micromachining process [22].

The BPF RF performance was characterised with an Agilent 8510 network analyser. Calibration planes were defined at the waveguide flanges, thus the loss because of the waveguide transitions is included in all measurements. The BPF was first measured without a MEMS tuner so as to evaluate the accuracy of the waveguide fabrication

doi: 10.1049/iet-map.2012.0722

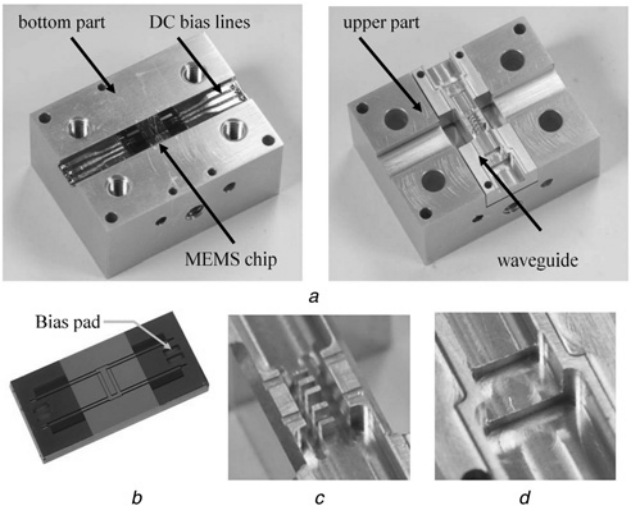

Fig. 6 *Manufactured prototypes*

a Manufactured prototype of the tuneable BPF. It consists of three metal parts (bottom part, upper part and waveguide) and a MEMS tuner
b MEMS tuner
c Detail of the evanescent-mode filter section comprising of five protruding studs
d Waveguide transition to a WR15 interface

process. A solid metal piece out of brass was utilised as the waveguide bottom wall. The BPF centre frequency was measured around 67.5 GHz (68 GHz in simulation), Fig. 3*b*. The in-band insertion loss and FBW were measured around 0.58 dB and 8.1%, respectively, and are in good agreement with the ones predicted by finite element simulations (IL: 0.5 dB and FBW:8%), Fig. 3*a*.

Later on, the MEMS tuner was integrated inside the waveguide bottom wall, Fig. 6. A 5-mil-thick dielectric substrate with Cu-metal printed lines on top of it was utilised for the DC biasing of the MEMS tuner, Fig. 6*a*. In such a way the DC biasing lines are out of the RF-signal path and do not contribute to the RF loss. The MEMS tuner was first glued on the substrate and wire bonded to the external DC biasing lines. The substrate was then mounted in the waveguide bottom wall and centred via optical alignment. The waveguide parts were coated with a very thin layer (<200 nm) of Au in order to facilitate the MEMS-chip and DC-bias circuitry mounting. Fig. 3*b* illustrates a comparison between the measured performance of a BPF with a solid brass bottom wall and a BPF with the MEMS tuner integrated inside the waveguide bottom wall. The effect of the MEMS tuner integration on the centre frequency (from 67.5 to 67.33 GHz) and FBW (from 8.1 to 8.3%) is negligible; whereas it considerably affects the in-band insertion loss (from 0.58 to 1.45 dB).

The measured reconfigurable performance of the BPF is presented in Fig. 5*c* and *d*. Various sets of biasing voltages ranging from 0 to 27.3 V corresponding to measured fingers deflections between 0.3 and 8.3° (characterised with a White Light Interferometer (WLI) prior to the RF measurement) were used for the filter characterisation. Although a finite number of states (state 1:0.3°, state 2: 4.5°, state 3: 6.5°, state 4: 7.5° and state 5: 8.3°) are shown; the centre frequency of the BPF can be tuned in an analogue manner from 67.4 to 63.2 GHz (4.2 GHz) by increasing the DC bias control voltage from 0 to 27.3 V. For this frequency band, the measured FBW varies between 8.3 (State 1:0 V) and 3.4% (State 5:27.3 V) and the in-band insertion loss between 1.45 and 5 dB, respectively.

A comparison between measured and simulated performance in terms of insertion loss, FBW and centre frequency is shown in Fig. 7. Aside from a small discrepancy in the insertion loss at the lower edge of the frequency band (e.g. ~1 dB loss excess at 63.8 GHz, if both performances are compared for the same centre frequencies); the measured RF performance is in a good agreement with the one obtained by finite element simulations. The measured centre frequency of the bandpass is slightly shifted to lower frequencies and the tuning range (4.2 GHz instead of 4 GHz) is slightly increased. These minor differences could be attributed to the dimensional tolerances of the waveguide metal parts (~±20 μm), discontinuities on the waveguide bottom wall because of the MEMS tuner integration (small gaps around 40 μm were measured between the MEMS element and the metal body), the assembly error and the material properties approximation used in simulation. Part of the reason of the excess of IL might be the leakage through the waveguide bottom wall since the assembly screws were not tightened enough to avoid breaking the MEMS tuner.

3.2 Long-term stability measurements

In order to examine the long-term behaviour of the BPF, its response was measured under constantly applied DC biasing voltages. The scattering parameters were recorded at various time steps starting from 10 to 1 h of operation. Two examples of two biasing states of 15 V and 25 V are shown in Fig. 8. It can be observed that the centre frequency of the bandpass moves towards lower frequencies with increasing time. In addition, the FBW reduces whereas insertion loss increases. Measured parameters follow an exponential curve that qualitatively agrees with the viscoelastic/creep characteristics demonstrated in [16, 23–26]. For example, with 25 V bias voltage, the frequency drift is −0.4% at the end of 420 sec and increases to −0.8% at the end of 2700 sec. In 1 h, the total drift is less than −0.83%.

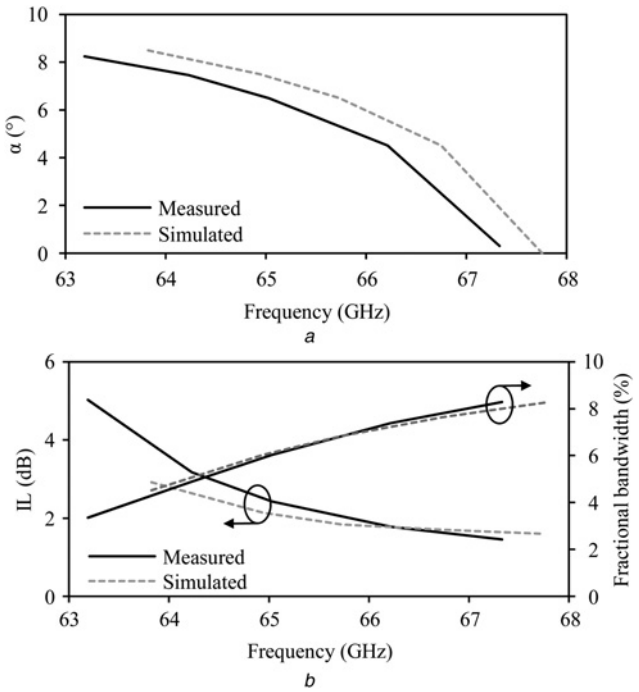

Fig. 7 *Comparison between simulated and measured performance, the illustrated parameters have been calculated from the responses shown in Fig. 5*

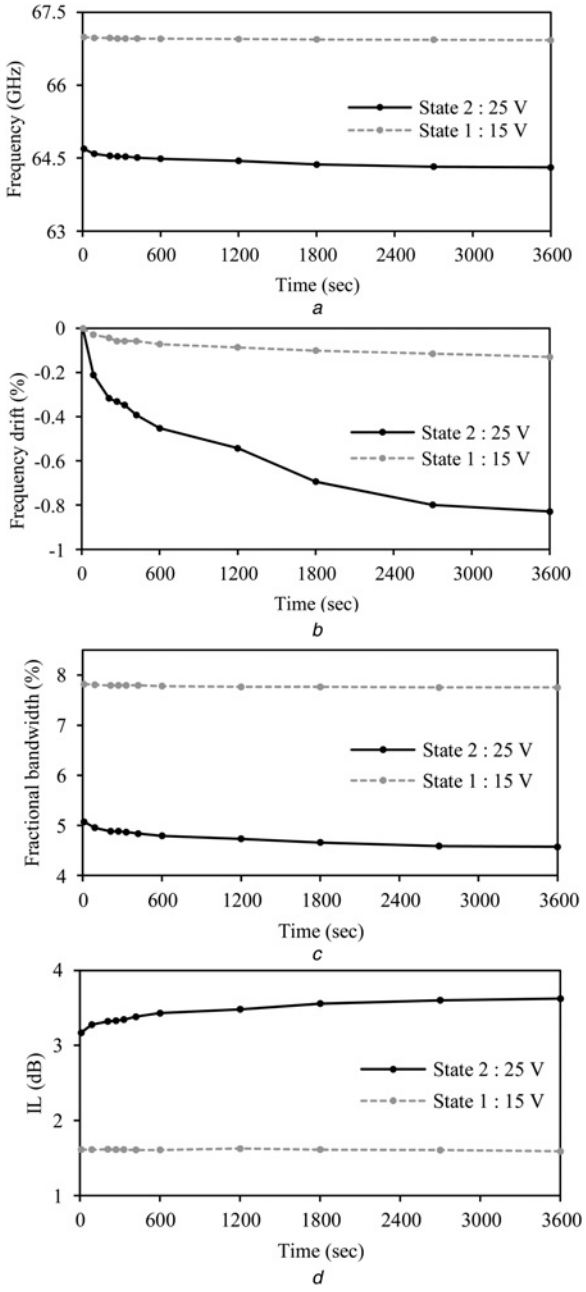

Fig. 8 *Long term measurements for two different biasing states: State 1: 15 V and State 2: 25 V*

Overall the BPF exhibits a small frequency drift and FBW drift. In particular for the 15 V state and after 1 h of operation; the centre frequency changes from 66.99 to 66.92 GHz (− 0.13%), the FBW from 7.82 to 7.75% (−0.9%) and the IL from 1.59 to 1.61 dB. For the 25 V state; the frequency drifts from 64.69 to 64.31 GHz (− 0.83%) and the FBW from 5.07 to 4.57% (− 9.86%). The drift appears to be higher for higher biasing levels because of the fact that the finger tips are closer to the resonator capacitive post (smaller capacitive gaps g_r) and are more sensitive to potential deflection variations. The deflection variation was characterised in a similar way (constantly applied bias voltage for 1 h) with the aid of a WLI and was found around 8.5% (from 2.7 to 2.93°) for the low biasing state and 6.3% (from 7.04 to 7.48°) for the high biasing state. It can be attributed to the viscoelastic nature of the polymer spring that results in creep when constant load is applied over time [23].

3.3 Comparison with the state-of-the-art

To the best of the authors' knowledge; the number of existing tuneable V-band BPFs is relatively limited because of the technological advances that the existing fabrication technologies would require so as to allow co-integration of tuning elements. A comparison between the proposed filter and alternative V-band tuneable BPFs reported in the literature is shown in Table 1. Illustrated topologies [2, 11–13] utilise implementation concepts that are based on planar transmission lines and MEMS capacitive membranes as tuning elements (MEMS cantilevers in [13]) and show low to moderate quality factors (24–68).

In this work, an implementation concept of a frequency reconfigurable BPF based on evanescent-mode waveguide resonators tuned by two highly conductive rigid fingers is reported for the first time. The proposed filter outperforms the one presented in [2] in terms of number of tuning elements (one instead of four), reconfigurable tuning states (analogue operation instead of two discrete states) and quality factor (68–108 instead of 24) whereas it occupies a large volume. The filters presented in [12, 13] exhibit higher dissipated power and require larger number of tuning elements (three and eight instead of one) than the filter shown in this study. In addition, although they have been initially-designed to be tuneable their reconfigurable operation has not yet been confirmed experimentally. Lastly, the tuning range and insertion loss of the proposed BPF are comparable with the ones of the analogue tuneable filter shown in [11]. However, the filter shown in this study requires fewer number of tuning elements (one instead of eight in [11]) and features a larger quality factor (68–108 instead of 25–30 in [11]). Finite element simulations showed that the average loss contribution because of the MEMS tuner can be improved by almost 1 dB if highly

Table 1 Comparison of V-band tuneable bandpass filters

	f_{cen}, GHz	BW, %	IL, dB	[a]Q_u	V, mm^3	N	Type
[2]	20–55	60–58	1.4 ± 0.2	24	2.8	4	digital
[11]	59–65.5	7.6–10.5	3.3 ± 0.2	25–30	0.7	8	analogue
[12]	59.7 [b](60.8–60.9)	9.8	3	68 [b](85–100)	5	3	static [b](analogue)
[13]	[c]63.4–64.9	N/A	[c]9.5 ± 0.2	[c]26–33	N/A	8	[c](analogue)
this work	63.2–67.4	3.4–8.3	3.2 ± 1.8	68–108	36[d]	1	analogue

N: Number of tuning elements, N/A: Not available
[a]Q_u extracted from measured data
[b]Tuning response of a single resonator
[c]Static measurements with non-actuated elements
[d]Volume calculated without the waveguide transition

doi: 10.1049/iet-map.2012.0722

doped Si is utilised (ρ: 0.0025 Ω·cm) and shows a potential in the realisation of a low loss tuneable BPF for V-band applications. A further improvement in terms of the overall filter loss is also expected if thick (5 × skin depth) metallisation coating (Au/Cu) is applied on the waveguide metal parts.

4 Conclusions

A MEMS-enabled BPF with continuously variable centre frequency is presented in this paper in terms of design and RF characterisation. The proposed concept is based on evanescent-mode capacitively loaded waveguide resonators tuned by MEMS actuated highly conductive rigid fingers directly integrated in the waveguide bottom wall. MEMS fingers deflections between 0.3 and 8.3° result in a centre frequency tuning between 67.4 and 63.2 GHz (4.2 GHz). For this frequency band the measured FBW varies between 8.3 and 3.4% and the in-band insertion loss is between 1.45 and 5 dB. An experimental study on the long term behaviour of the BPF response under constantly applied DC bias voltage for 1 h of operation was performed and showed a small centre frequency drift ($< -0.83\%$) and FBW drift ($< -9.86\%$).

5 Acknowledgments

This work has been supported by the Swiss National Science Foundation (SNF) under grant 200021_129832. The authors thank Professor C. Hierold for the fruitful discussions and H.-R. Benedickter and M. Lanz for their technical support.

6 References

1 Lucyszyn, S.: 'Advanced RF MEMS' (Cambridge University Press, Cambridge, 2010)
2 Park, J.-H., Lee, S., Kim, J.-M., Kim, H.-T., Kwon, Y., Kim, Y.-K.: 'Reconfigurable millimeter-wave filters using CPW-based periodic structures with novel multiple-contact MEMS switches', *IEEE J. Microelectromech. Syst.*, 2005, **14**, (3), pp. 456–463
3 Hsu, C.-Y., Chen, C.-Y., Chuang, H.-R.: 'A 60 GHz millimeter-wave bandpass filter using 0.18-μm CMOS technology', *IEEE Electron. Device Lett.*, 2008, **29**, (3), pp. 246–248
4 Huang, P.-L., Chang, J.-F., Lin, Y.-S., Lu, S.-S.: 'Micromachined V-band CMOS bandpass filter with 2 dB insertion loss', *IET Electron. Lett.*, 2008, **45**, (2), pp. 100–101
5 Nan, L., Mouthaan, K., Xiong, Y.-Z., Shi, J., Rustagi, S.C., Ooi, B.-L.: 'Design of 60- and 77-GHz narrow-bandpass filters in CMOS technology', *IEEE Trans. Circuits Syst. II: Express Briefs*, 2008, **55**, (8), pp. 738–742
6 Choi, S.T., Yang, K.S., Tokuda, K., Kim, Y.H.: 'A V-band planar narrow bandpass filter using a new type integrated waveguide transition', *IEEE Microw. Wirel. Compon. Lett.*, 2004, **14**, (12), pp. 545–547
7 Bairavasubramanian, R., Pinel, S., Laskar, J., Papapolymerou, J.: 'Compact 60-GHz bandpass filters and duplexers on liquid crystal polymer technology', *IEEE Microw. Wirel. Compon. Lett.*, 2006, **16**, (5), pp. 237–239
8 Hsiao, C.-Y., Hsu, S.S.H., Chang, D.-C.: 'A compact V-band bandpass filter in IPD technology', *IEEE Microw. Wirel. Compon. Lett.*, 2011, **21**, (10), pp. 531–533
9 Lee, J.-H., Pinel, S., Papapolymerou, J., Laskar, J., Tenzeris, M.M.: 'Low-loss LTCC cavity using system-on-package technology at 60 GHz', *IEEE Trans Microw. Theory Tech.*, 2005, **53**, (12), pp. 3817–3824
10 Mruk, J.R., Filipovic, D.S.: 'Micro-coaxial V-/W-band filters and contiguous diplexers', *IET Microw. Antennas Propag.*, 2012, **6**, (10), pp. 1142–1148
11 Kim, H.-T., Park, J.-H., Kim, Y.-K.: 'Low-loss and compact V-band MEMS-based analog tunable bandpass filters', *IEEE Microw. Wirel. Compon. Lett.*, 2002, **12**, (11), pp. 432–434
12 Lucyszyn, S., Miyaguchi, K., Jiang, H.W., *et al.*: 'Micromachined RF-coupled inverted-microstrip millimeter-wave filters', *IEEE J. Microelectromech. Syst.*, 2008, **17**, (3), pp. 767–776
13 Seok, S., Kim., J., Rolland, N., Rolland, P.-A.: 'A study on millimeter-wave tunable bandpass filter based on polymer cap deflection', *Micromachines*, 2012, **3**, (1), pp. 28–35
14 Park, S.-J., Reines, I., Patel, C., Rebeiz, G.M.: 'High-Q RF-MEMS 4–6-GHz tunable evanescent-mode cavity filter', *IEEE Trans. Microw. Theory Tech.*, 2010, **58**, (2), pp. 381–389
15 Amadjikpe, A.L., Chung, D.J., Courreges, S., Eudeline, P., Ziaei, A., Papapolymerou, J.: 'Two-pole digitally tunable evanescent-mode waveguide narrow-band filter with radio frequency micro-electromechanical systems switches', *IET Microw. Antennas Propag.*, 2011, **5**, (4), pp. 393–401
16 Liu, X., Katehi, L.P.B., Chappell, W.J., Peroulis, D.: 'High-Q tunable microwave cavity resonators and filters using SOI-based RF MEMS tuners', *IEEE Trans. Microw. Theory Tech.*, 2010, **19**, (4), pp. 774–784
17 Arif, M.S., Peroulis, D.: 'A 6 to 24 GHz continuously tunable, microfabricated, high-Q cavity resonator with electrostatic MEMS actuation', IEEE MTT-S Int. Microwave Symp. on Tech. Digest, 2012, pp. 1–3
18 Matthaei, G.L., Young, L., Jones, E.M.T.: 'Microwave filters, impedance-matching networks and coupling structures' (McGraw-Hill Book Company, New York, NY, 1964)
19 Craven, G.F., Mok, C.K.: 'The design of evanescent mode waveguide bandpass filters for a predescribed insertion loss characteristic', *IEEE Trans. Microw. Theory Tech.*, 1971, **19**, (3), pp. 295–308
20 Psychogiou, D., Hesselbarth, J., Li, Y., Kühne, S., Hierold, C.: 'W-band tunable reflective type phase shifter based on waveguide-mounted RF MEMS', IEEE MTT-S Int. Microwave Workshop Series on Millimeter Wave Integration Technologies, 2011, pp. 85–88
21 Psychogiou, D., Li, Y., Hesselbarth, J., *et al.*: 'Millimeter-wave phase shifter based on waveguide-mounted RF-MEMS', *Microw. Opt. Technol. Lett.*, 2013, **53**, (3), pp. 465–468
22 Li, Y., Kühne, S., Psychogiou, D., Hesselbarth, J., Hierold, C.: 'A microdevice with large deflection for variable-ratio RF MEMS power divider applications', *J. Micromech. Microeng.*, 2011, **21**, (7), p. 074013
23 Schoeberle, B., Wendlandt, M., Hierold, C.: 'Long-term creep behavior of SU-8 membranes: application of the time-stress superposition principle to determine the master creep compliance curve', *Sens. Actuators A, Phys.*, 2008, **142**, pp. 242–249
24 Yan, X., Brown, W.L., Li, Y., *et al.*: 'Anelastic stress relaxation in gold films and its impact on restoring forces in MEMS devices', *J. Microelectromech. Syst.*, 2009, **18**, (3), pp. 570–576
25 Hsu, H.-H., Koslowski, M., Peroulis, D.: 'An experimental and theoretical investigation of creep in ultrafine crystalline nickel RF-MEMS devices', *IEEE Trans. Microw. Theory Tech.*, 2011, **59**, (10), pp. 2655–2664
26 Hsu, H.-H., Peroulis, D.: 'A CAD model for creep behaviour of RF-MEMS varactors and circuits', *J. Microelectromech. Syst.*, 2011, **59**, (3), pp. 1761–1768